Earth and Planetary Science Letters 385 (2014) 89–96

Contents lists available at ScienceDirect

Earth and Planetary Science Letters

www.elsevier.com/locate/epsl

Rupture complexity of the 1994 Bolivia and 2013 Sea of Okhotsk deep earthquakes

Zhongwen Zhan *, Hiroo Kanamori, Victor C. Tsai, Donald V. Helmberger, Shengji Wei

Seismological Laboratory, California Institute of Technology, 1200 E. California Blvd., Pasadena, CA 91125, USA

ARTICLE INFO

Article history:
Received 14 October 2013
Accepted 19 October 2013
Available online xxxx
Editor: Y. Ricard

Keywords:
deep earthquake
earthquake rupture
body wave

ABSTRACT

The physical mechanism of deep earthquakes (depth >300 km) remains enigmatic, partly because their rupture dimensions are difficult to estimate due to their low aftershock productivity and absence of geodetic or surface rupture observations. The two largest deep earthquakes, the recent Great 2013 Sea of Okhotsk earthquake (M 8.3, depth 607 km) and the Great 1994 Bolivia earthquake (M 8.3, depth 637 km), together provide a unique opportunity to compare their rupture patterns in detail. Here we extend a travel-time sub-event location method to perform full teleseismic P-waveform inversion. This new method allows us to explain the observed broadband records with a set of sub-events whose model parameters are robustly constrained without smoothing. We find that while the Okhotsk event is mostly unilateral, rupturing 90 km along strike with a velocity over 4 km/s, the Bolivia earthquake ruptured about half this distance at a slow velocity (about 1.5 km/s) and displayed a major change in rupture direction. We explain the observed differences between the two earthquakes as resulting from two fundamentally different faulting mechanisms in slabs with different thermal states. Phase transformational faulting is inferred to occur inside the metastable olivine wedge within cold slab cores whereas shear melting occurs inside warm slabs once triggered.

1. Introduction

Several mechanisms for deep earthquakes have been proposed, including thermal shear instability (Ogawa, 1987; Kanamori et al., 1998; Karato et al., 2001), dehydration embrittlement of pre-existing faults (Meade and Jeanloz, 1991; Silver et al., 1995), and transformational faulting associated with a metastable olivine wedge in cold subducting slabs (Green and Burnley, 1989; Kirby et al., 1991, 1996; Green and Houston, 1995). These mechanisms have been previously evaluated using deep earthquake rupture properties (e.g., duration, rupture dimension, rupture speed, stress drop, and radiation efficiency; Wiens, 2001; Tibi et al., 2003; Suzuki and Yagi, 2011), aftershock statistics (Wiens, 2001; Houston, 2007), and their depth dependence (Persh and Houston, 2004a, 2004b; Tocheport et al., 2007). Among these mechanisms, phase transformational faulting and thermal shear instability, possibly involving melting, have so far garnered the most evidence (Wiens, 2001; Houston, 2007). It has also been suggested that deep earthquake mechanisms may depend on the thermal state of the subducting slab (Wiens and McGuire, 1995; Wiens and Gilbert, 1996; Wiens, 2001; Tibi et al., 2003; Houston, 2007), but evidence has been inconclusive (Suzuki and Yagi, 2011).

The 1994 Bolivia earthquake was the largest deep earthquake until the recent 2013 Okhotsk earthquake of similar magnitude (Fig. 1), and has provided critical information about deep earthquake mechanisms. The earthquake was previously characterized by low rupture speed (~1.5 km/s), high static stress drop, and low radiation efficiency (e.g., Kikuchi and Kanamori, 1994; Silver et al., 1995; Ihmlé, 1998). The earthquake's rupture dimension (~30 km × 40 km) is small for its size, yet significantly larger than the predicted width of the metastable olivine wedge (Tibi et al., 2003), unless significant thickening of the slab occurs due to plate bending (Kirby et al., 1995). Kanamori et al. (1998) suggest instead that shear melting could have promoted extensive sliding with high energy dissipation which resulted in large slip, high stress drop and slow rupture speed.

The 2013 Okhotsk deep earthquake was of similar size as the Bolivia earthquake, but occurred in a different tectonic setting. The subducted Pacific plate in which the Okhotsk earthquake occurred is significantly older and hence colder than the subducted Nazca plate in which the Bolivia earthquake occurred (Wiens and Gilbert, 1996). A thorough comparison of these two earthquakes' rupture properties thus provides important constraints on the faulting

* Corresponding author now at: Institute of Geophysics and Planetary Physics, Scripps Institution of Oceanography, University of California, San Diego, 9500 Gilman Dr., La Jolla, CA 92093-0225, USA. Tel.: +1 858 534 1543.
E-mail addresses: zwzhan@ucsd.edu, zwzhan@gmail.com (Z. Zhan).

0012-821X/$ – see front matter
http://dx.doi.org/10.1016/j.epsl.2013.10.028

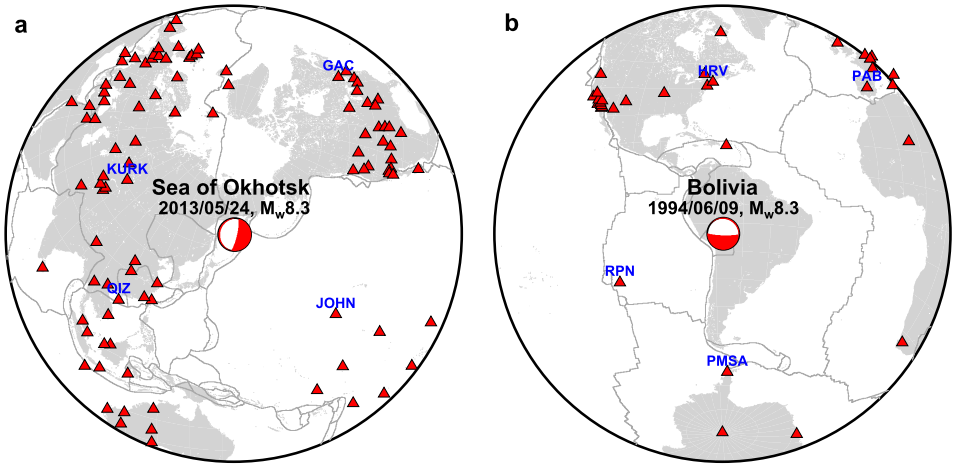

Fig. 1. Earthquake and station locations. Teleseismic stations used to study **(a)** the 2013/05/24 M_w 8.3 Okhotsk earthquake, and **(b)** the 1994/06/09 M_w 8.3 Bolivia earthquake.

mechanism of deep earthquakes and its temperature dependence. We note that recently Ye et al. (2013) and Wei et al. (2013) report rupture models of the 2013 Okhotsk earthquake using finite-fault inversions and back-projections. They also make brief qualitative comparisons with previously published rupture processes of the 1994 Bolivia earthquake (e.g., Kikuchi and Kanamori, 1994; Silver et al., 1995; Ihmlé, 1998). In contrast, this paper emphasizes the development of a new sub-event method, and the application of this method to both the Okhotsk and Bolivia earthquakes. With source parameters seismologically constrained by the same methodology, we are able to make more thorough comparisons between the Okhotsk and Bolivia earthquakes, and discuss the fundamental difference in rupture physics.

2. Data and methods

We follow a two-step approach to obtain the sub-event models of the two deep earthquakes. We first conduct a directivity analysis to infer the qualitative rupture properties, including the major rupture directions, approximate number of sub-events, and their origin times and locations. We then use these results as a starting model for each earthquake and apply the sub-event method to obtain the final sub-event models.

Fig. 1 shows the teleseismic stations that we use for analysis of the 1994 Bolivia earthquake and the 2013 Okhotsk earthquake. We use all broadband vertical-component data available from IRIS for the two earthquakes, removing instrument responses to obtain broadband displacement records. Then, to avoid complicated waveforms caused by 3D structure, we eliminate stations with poor data quality near the GCMT moment tensor nodal planes (Ekström et al., 2012). For the Okhotsk earthquake, we further downsample the data to keep only the station with the highest signal-to-noise ratio in each 1 degree of azimuth, which avoids heavily weighting azimuths with very dense networks (e.g., US and Europe). Since the Bolivia earthquake had much sparser data coverage, we keep as many stations as possible to ensure good azimuthal coverage. For all remaining stations, we flip the P-wave polarities to be positive only, and hand-pick the P-wave first arrivals as the reference times for the following analyses.

2.1. Directivity analysis

Earthquake source dimension and rupture directivity directly affect the azimuth and distance dependence of waveforms. This dependence is easily quantified for an earthquake that consists of a few sub-events (e.g., Silver et al., 1995; Ammon et al., 2005). For the n-th sub-event at time T_n with distance L_n from the hypocenter, the timing of the observed P-wave displacement pulse at any station i can be written as

$$T_n^i = T_n - \frac{L_n}{c_P^i}\cos\left(\theta_i - \theta_r^n\right), \tag{1}$$

where θ_i is the station azimuth, θ_r^n is the rupture direction, and c_P^i is the phase velocity of the teleseismic P wave (which depends on station distance). Defining a directivity parameter following Ammon et al. (2005), $x_i = -\frac{\cos(\theta_i - \theta_r^n)}{c_P^i}$, then $T_n^i = T_n + L_n \cdot x_i$. Therefore, arranging teleseismic P waves by directivity parameter $x_i(\theta_r^n)$, different sub-events can be identified as different straight lines with slope L_n and zero-crossing point at T_n. The choice of rupture direction θ_r^n is based on trial and error, and could be different for different sub-events.

Teleseismic P waveforms for the Okhotsk earthquake (Fig. 2a) show strong directivity to the NNW and SSE (N165°E), with a few major sub-events clearly visible in the directivity plot. Unlike for the Okhotsk earthquake, waveforms of the Bolivia earthquake cannot be aligned well with a single rupture direction, and require two rupture stages (Fig. 2b, c). In stage 1, the Bolivia earthquake ruptured to the east with a series of small sub-events, whereas in stage 2 the rupture grew rapidly and the last sub-event arrival is better fit with rupture to the NE. For each well-aligned major P wave arrival, we define a sub-event, and measure the slope to determine its distance from the epicenter, as displayed in the insets of Fig. 2. The origin times and locations of these sub-events are used as starting models in the more quantitative sub-event analysis.

2.2. Sub-event method

While the essential features of both the Okhotsk and Bolivia earthquakes are easily visualized in the directivity plots of Fig. 2, quantitative details regarding the precise locations and timings of the sub-events cannot be determined from visual inspection. We therefore introduce a new sub-event algorithm to simultaneously invert broadband P waveforms for multiple sub-events' centroid locations, centroid times and moments. This algorithm is based on previous sub-event modeling (Kikuchi and Kanamori, 1991; Tsai et al., 2005; Duputel et al., 2012), but does not require the subjective hand picking of coherent arrivals. Given a set of sub-event locations and times, we first predict the sub-event arrival times for each station. We then assume Gaussian-shaped source-time-functions centered at the predicted arrival times and invert

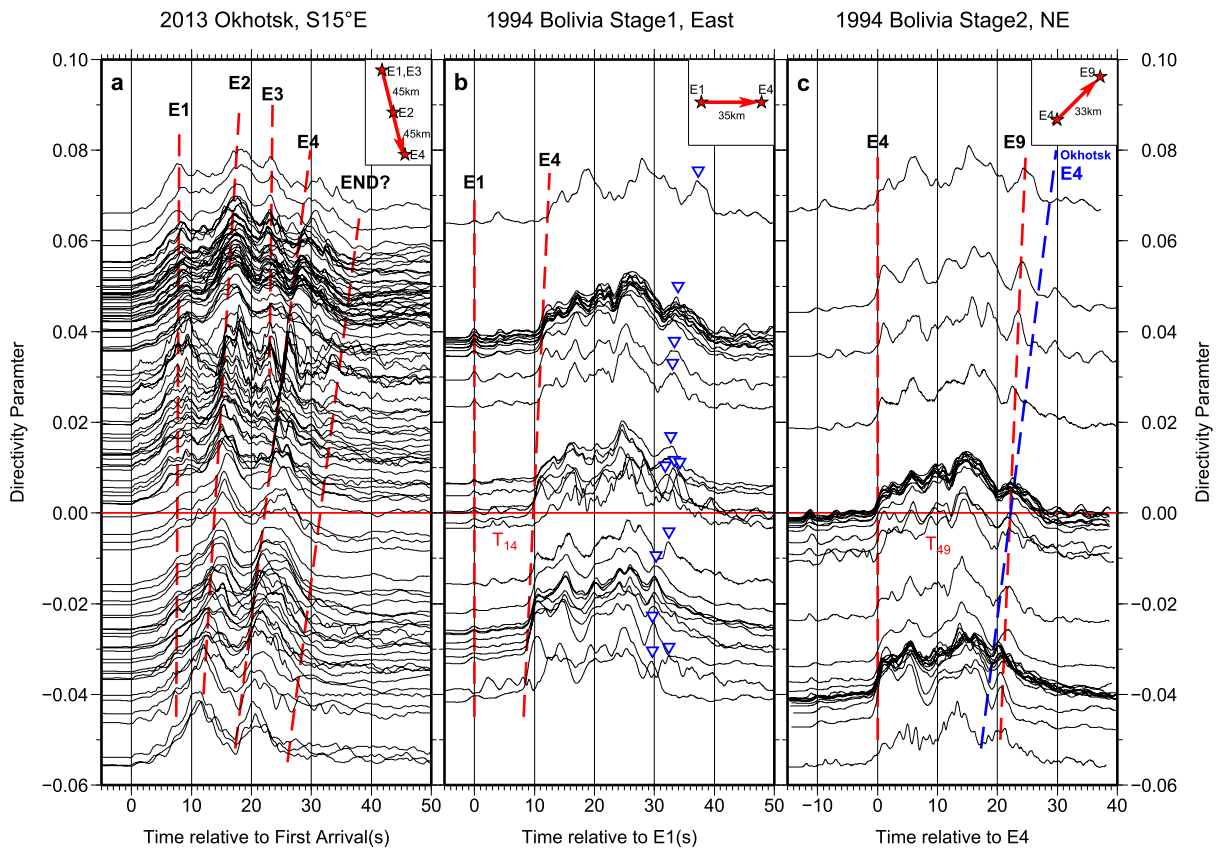

Fig. 2. Rupture directivity. Directivity plots for the broadband teleseismic P waves from the Okhotsk and Bolivia earthquakes. Since we do not invert for focal mechanisms here, we flip the P-wave polarities to be positive only, while keeping the true amplitudes. **(a)** Teleseismic P waves from the Okhotsk earthquake arranged by directivity parameter, assuming rupture direction towards S15°E and aligned by hand-picked first arrivals. We identify four major sub-events (E1, E2, E3 and E4) and the approximate end (END) marked by the red dashed lines, whose slopes are controlled by their distances from the epicenter. The times of the dashed lines at directivity parameter 0.00 identify the times of the sub-events from the earthquake origin time. The inset shows the approximate relative locations of E1, E2, E3 and E4. **(b)** Similar to (a) but for the Bolivia earthquake stage 1, assuming rupture direction to the east. Due to the non-emergent first arrivals, the waveforms are aligned by the first sub-event E1. Sub-event E4 denotes the sharp rise of P-wave amplitudes, is well aligned, and its time from E1 is denoted as T_{14}. The blue inverted triangles show that arrivals from the last major sub-event E9 are not well aligned by directivity to the east. **(c)** Similar to (b) but for the Bolivia earthquake stage 2, assuming rupture to the north–east. The P waveforms are aligned by sub-event E4. The last major sub-event E9 is delayed by T_{49} relative to E4, and is marked by a red dashed line. For comparison, the Okhotsk sub-event E4 from panel (a) is shown as a blue dashed line. The similar timing but steeper slope of the Bolivia E9 compared to the Okhotsk E4 suggests that the Bolivia earthquake has smaller rupture dimension and lower average speed than the Okhotsk earthquake. (For interpretation of the references to color in this figure legend, the reader is referred to the web version of this article.)

the waveform data for the best fitting durations and amplitudes for each station independently to accommodate radiation patterns, and path and site effects. Sub-event amplitudes and durations are assumed to be the average of the individual station amplitudes and durations, respectively.

We use an iterative nonlinear least squares algorithm similar to Tsai et al. (2005) to iteratively update the sub-event locations and times by minimizing waveform misfit. The choice of starting points and the number of sub-events can be adjusted based on waveform misfit and directivity analysis. The procedure requires initial guesses for sub-event model parameters, and we use our visually-determined results of the directivity analyses for both the Okhotsk and Bolivia earthquakes (plus published results for the Bolivia earthquake, e.g., Kikuchi and Kanamori, 1994; Silver et al., 1995; Ihmlé, 1998), so that convergence is reached within a few iterations. To test the robustness of the final solutions, we also perturb the initial models (by as much as 20 km in location and 10 s in time), and the majority of the results converge to the same models within 20 iterations. Significant initial perturbations which lead to very different solutions or even divergences can be visually identified to have much worse waveform fits, and all have higher total misfits than our preferred solution.

As with other sub-event methods (Kikuchi and Kanamori, 1991; Tsai et al., 2005; Duputel et al., 2012), we use only a small number of sub-events with a correspondingly small number of free parameters; yet our method can explain the observed broadband data with sufficient detail to estimate both the spatial and temporal moment distribution. Due to the small number of parameters estimated, our sub-event inversion does not require damping, smoothing or constraints on rupture velocity. Our method also uses global broadband data, rather than the regional high-frequency data of back-projection methods (Ishii et al., 2005), and therefore resolves the broadband slip distribution.

3. Sub-event models

Fig. 3a, b and Tables S1 and S2 describe the final sub-event models for the Okhotsk and Bolivia earthquakes, respectively, where sub-event moments are assumed to be proportional to the average observed P-wave amplitudes. Waveforms are generally well fit (Fig. 3c, d and Fig. S1) and the sub-event models confirm the first-order features revealed by the directivity analysis.

3.1. The Okhotsk earthquake

The Okhotsk earthquake first ruptured sub-event E1 slightly to the NE of the epicenter at about 8 s, then proceeded to the south and ruptured its biggest sub-event E2. Perhaps due to the large

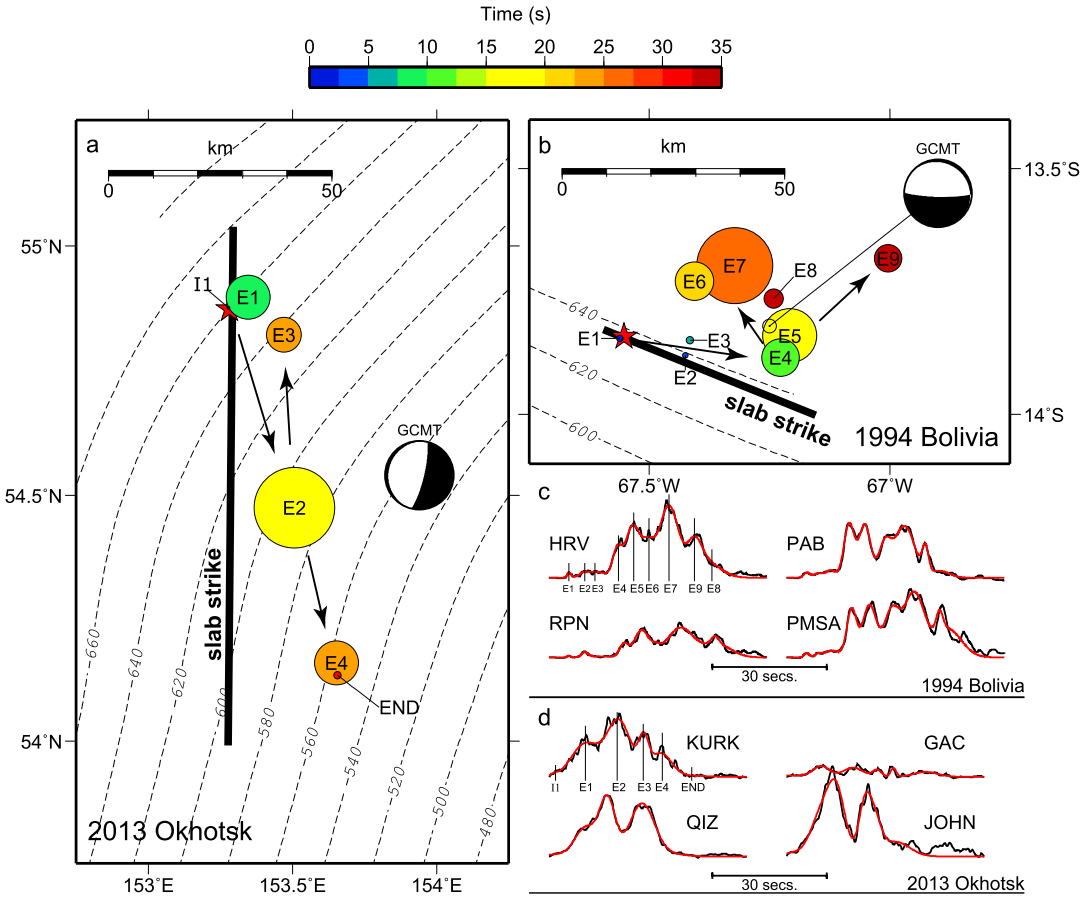

Fig. 3. Sub-event models of **(a)** the Okhotsk earthquake, and **(b)** the Bolivia earthquake. The red stars are the USGS NEIC epicenters, used as the reference starting points. Circles represent the earthquake sub-events with moments denoted by the sizes of the circles, and colors indicating sub-event centroid times. The black arrows illustrate the approximate rupture sequences. Slab strikes derived from aftershock distributions are displayed as thick black lines (see Fig. 4 for the Okhotsk sequence, and Myers et al. (1995) for the Bolivia sequence). Slab contours from the Slab 1.0 model (Hayes et al., 2012) are shown as dashed lines, and the differences from the thick black line for the Okhotsk earthquake is discussed in Fig. 4. The N-axes of the Global CMT solutions of both earthquakes are approximately aligned with their respective slab strikes. **(c)** and **(d)** show example waveform fits for the sub-event models, for the Bolivia and Okhotsk earthquakes, respectively, with observed waveforms in black and predicted waveforms in red. The stations shown here are highlighted in Fig. 1, and are representative of different azimuths. On the first example for each earthquake, the predicted arrival times of sub-events are marked by thin vertical lines. The complete waveform fits can be found in Fig. S1. (For interpretation of the references to color in this figure legend, the reader is referred to the web version of this article.)

slip, the rupture reset to propagate both north and south, generating E3 back near the epicenter (between E1 and E2) and E4 to the south. Finally, the rupture ended towards E4 at about 30 s (see Fig. 3a and Fig. 2a). From the hypocentral time to the onset of E4, the overall rupture speed was over 4 km/s, about 70% of the shear wave velocity (~5.5 km/s) at 607 km depth. The overall rupture was about 90 km long in the N165°E direction, and was aligned roughly with the N-axis of the Okhotsk earthquake's GCMT focal mechanism (Ekström et al., 2012) as well as being fairly close to the slab strike derived from the aftershock distribution (thick black line in Fig. 3a and Fig. 4).

The amplitudes and durations from the sub-event modeling provide constraints on each sub-event's focal mechanism and directivity, and also on path and site effects. In principle, we could invert for each sub-event's focal mechanism, given certain assumptions about directivity and path/site effects. Instead, we compare the amplitude patterns of different sub-events to test whether there is any clear difference in focal mechanism, and find that all sub-events have radiation patterns that are largely consistent with each other (Fig. 5). This consistency in radiation patterns suggests a relatively uniform faulting geometry along the entire Okhotsk earthquake rupture. Sub-event E3's radiation pattern is hard to constrain because of its small amplitude and strong interference with E4. Sub-event E4 has slightly stronger radiation to the south–west direction compared to E1 and E2, but this may also be caused by interference with E3.

3.2. The Bolivia earthquake

The Bolivia earthquake started with a 10-s-long weak but fast (3.5 km/s, 60–70% of the shear wave velocity) eastward rupture and generated three small sub-events (E1, E2 and E3) and a large sub-event E4 (stage 1). In stage 1, the rupture was approximately aligned with the N-axis of the Bolivia earthquake's GCMT focal mechanism (Ekström et al., 2012) as well as the slab strike from the aftershock distribution (Myers et al., 1995) and Slab 1.0 (Hayes et al., 2012) (thick and dashed lines in Fig. 3b, respectively). Similar to what occurred after E2 of the Okhotsk earthquake, after E4, the Bolivia rupture also reset and changed rupture direction. However, rather than continuing along the slab strike, the rupture progressed to the north and NNW with E5, E6, E7, E8 and to the NE with E9. Most of the slip occurred during this stage. This main rupture area was about 30 km × 40 km, and lasted about 22 s, characterizing a slow rupture speed of about 1.5 km/s (about 30% of the shear wave velocity). Our sub-event model for the Bolivia earthquake is roughly consistent with previous studies (e.g., Kikuchi and Kanamori, 1994; Silver et al., 1995; Ihmlé, 1998; Fig. S2).

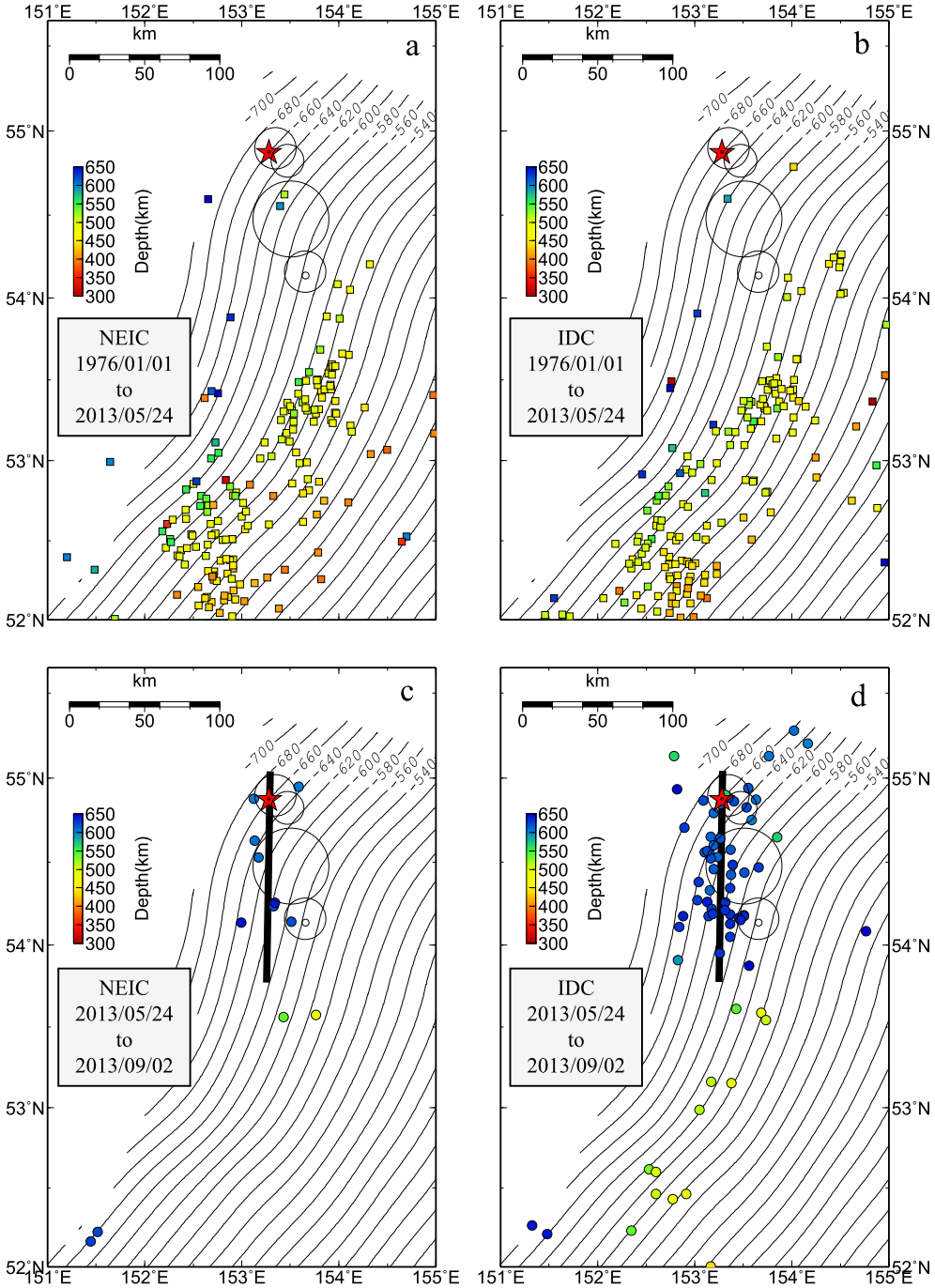

Fig. 4. Seismicity before and after the 2013 Okhotsk earthquake, and slab geometry. **(a)** and **(b)** show the seismicity from 1976/01/01 to 2013/05/24 before the Okhotsk earthquake, reported by the National Earthquake Information Center (NEIC) and International Data Centre (IDC), respectively. **(c)** and **(d)** show the seismicity after the Okhotsk earthquake, reported by the NEIC and IDC, respectively. The red stars are the NEIC epicenters. Circles represent the earthquake sub-events. Slab contours from the Slab 1.0 model are shown as thin black lines. As shown in (a) and (b), there were only a few earthquakes near the Okhotsk earthquake beforehand, so we conclude that the slab geometry of Slab 1.0 may not be accurate near the Okhotsk earthquake. Instead, the aftershock sequence shown in (c) and (d) forms a roughly north–south trend (thick black lines). If we assume that deep earthquakes nucleate inside the slab cold core, then we can approximate the slab strike by the trend of aftershocks. This new, preferred slab strike is significantly different than that of Slab 1.0. (For interpretation of the references to color in this figure legend, the reader is referred to the web version of this article.)

3.3. Ruptures on sub-horizontal fault planes

In our analysis, we initially do not use constraints on sub-event locations and, in particular, we make no assumptions about sub-event depths. Since our data has good azimuthal coverage, we find that sub-event depths have tradeoffs only with sub-event timings and not with the sub-event horizontal locations, which are well determined from the azimuthal dependencies of the data. For the Bolivia earthquake, our sub-event horizontal locations are broadly consistent with the sub-horizontal rupture of previous studies (e.g., Kikuchi and Kanamori, 1994; Silver et al., 1995; Ihmlé, 1998; Fig. S2) and, moreover, our observed spread in sub-event locations (Fig. 3b) is inconsistent with rupture along a single near-vertical GCMT fault plane in the east–west direction. We therefore assume horizontal rupture, consistent with rupture along the near-horizontal GCMT fault plane. Similarly, our sub-event locations for the Okhotsk earthquake (Fig. 3a) are roughly aligned with azimuth of −15°, inconsistent with rupture on the near-vertical

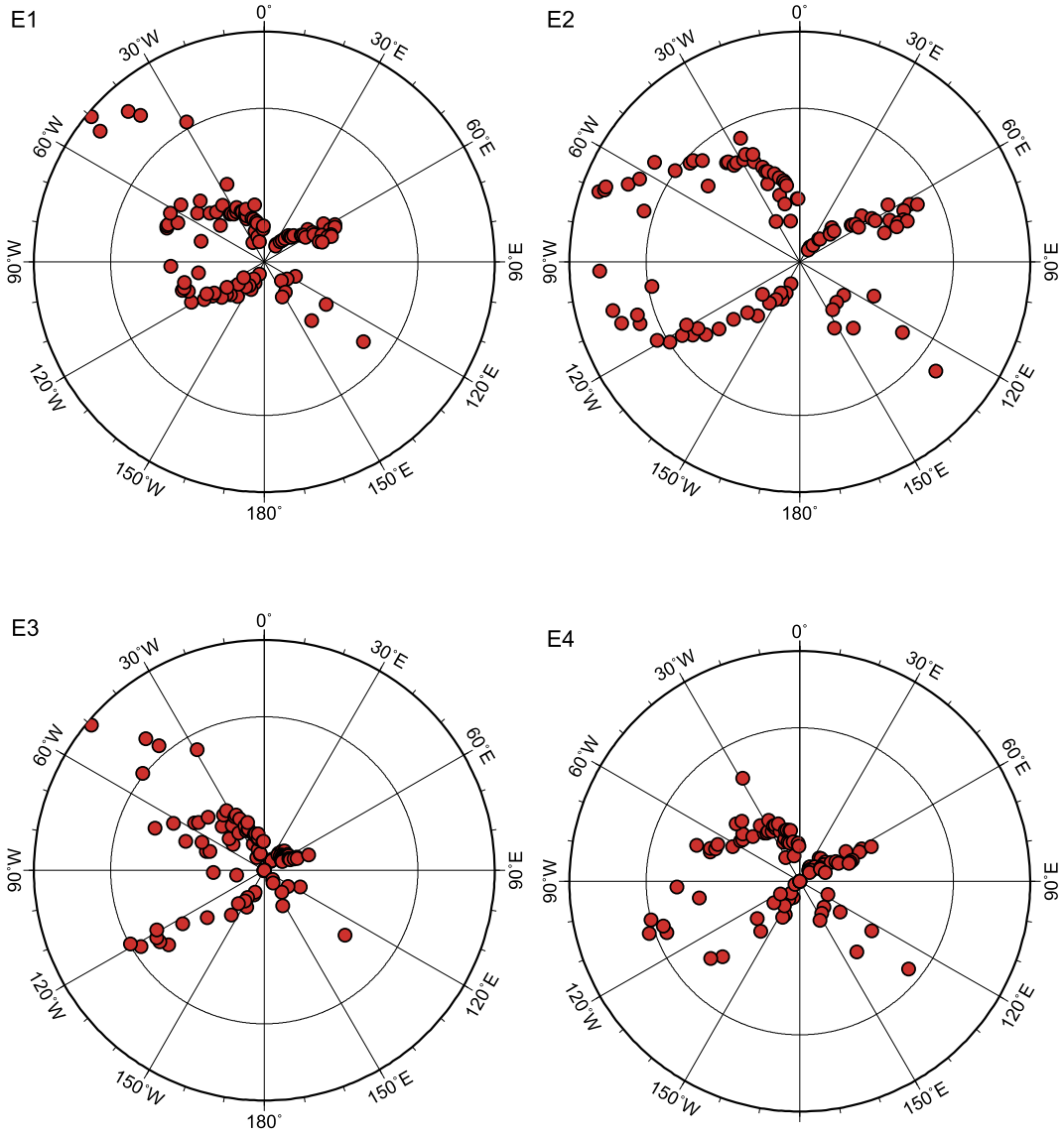

Fig. 5. Radiation patterns of sub-events E1, E2, E3 and E4 of the 2013 Okhotsk earthquake. The red dots display different sub-events' amplitudes at different stations, including the contributions from focal mechanisms, directivity, path and site effects. The four sub-events have radiation patterns that are largely consistent with each other, suggesting a relatively uniform faulting geometry along the entire rupture.

GCMT fault plane with strike of 12°, but consistent with rupture on the near-horizontal GCMT fault plane, and we therefore also assume horizontal rupture. To test this assumption, we conduct finite-fault inversions with both fault planes of the GCMT solution, and find that waveforms are significantly better fit with the sub-horizontal fault plane (Fig. S3, Fig. S4, and Fig. S5). The assumption of sub-horizontal rupture is further supported by mainshock and aftershock depths. The Okhotsk earthquake GCMT centroid depth is 607 km, very close to the hypocenter depths from the National Earthquake Information Center (NEIC) catalog (608.9 km). A number of aftershocks (Fig. 4) located by the NEIC and International Data Centre (IDC)/Comprehensive Nuclear-Test-Ban Treaty Organization (CTBTO) are also roughly in a horizontal plane with a similar depth (scattered between 590 and 640 km, with a mean of 620 km based on IDC/CTBTO) as the Okhotsk mainshock (International Seismological Centre, 2011).

In short, although the Bolivia earthquake and the Okhotsk earthquake have similar depths and moments, they have significantly different rupture processes and geometries. We find that the Okhotsk earthquake is twice as long and has rupture speed twice as high as the Bolivia earthquake. This implies that the Okhotsk earthquake has significantly lower static stress drop and higher radiation efficiency than the Bolivia earthquake. The two earthquakes' major ruptures also have different orientations with respect to the N-axes of the focal mechanisms and the local slab strikes. Additionally, both earthquakes show well-resolved dynamic rupture processes strongly affected by sub-events with large slip.

4. Discussion and conclusions

The new rupture models obtained here have significant implications for the mechanics of deep earthquakes. Previous studies (Wiens, 2001; Tibi et al., 2003), using sets of large deep earthquakes ($M > 7$), have observed slow rupture velocities for events in warm subduction zones, such as the South American subduction zone, and fast rupture velocities in cold subduction zones like Tonga. Although speculative, it has been suggested that two fundamentally different faulting mechanisms might operate for deep earthquakes (Green and Burnley, 1989; Kirby et al., 1991). For the two largest deep earthquakes studied in this paper, the Bolivia

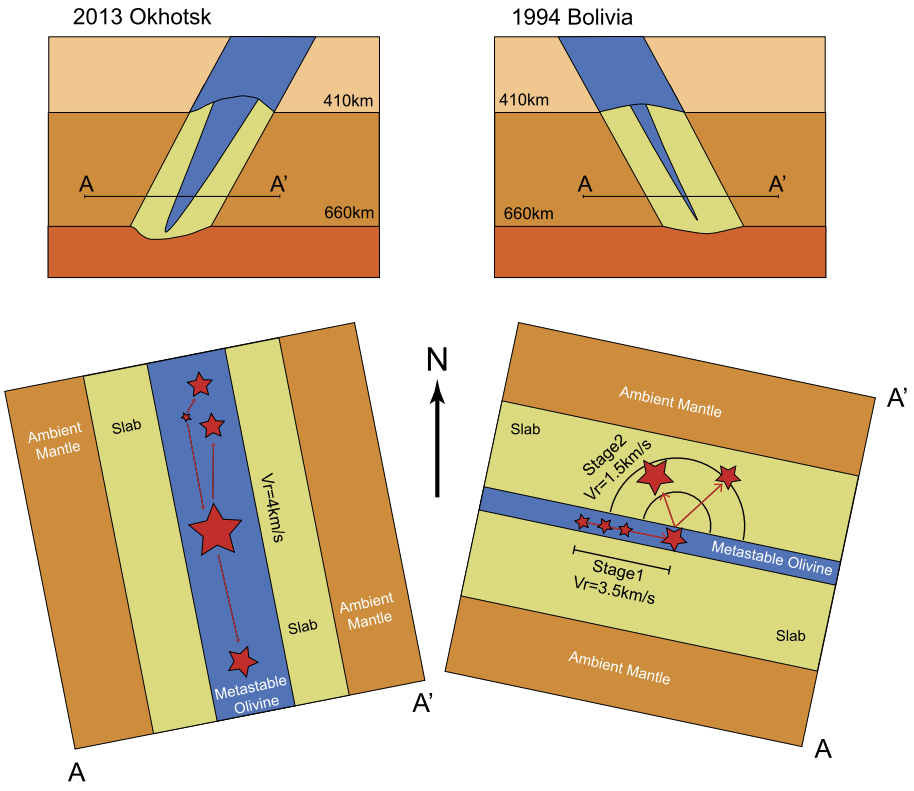

Fig. 6. Conceptual models of the Okhotsk and Bolivia earthquakes in cross section (top panels) and map view (bottom panels). Due to differences in the thermal states of the subducting slabs in which the two earthquakes occurred, the widths of the metastable olivine wedges in the slab cores are also different. This causes different dominant faulting mechanisms for the two largest deep earthquakes. The Okhotsk earthquake is inferred to have ruptured mostly inside the relatively thick metastable olivine wedge, whereas the Bolivia earthquake's major rupture, stage 2, was outside the relatively thin metastable olivine wedge. See the main text for details.

earthquake occurred in the relatively warm South American subduction zone, whereas the Okhotsk earthquake occurred in the relatively cold Kuril subduction zone (Wiens and Gilbert, 1996). We find that they have significantly different source dimension, rupture speed, and orientation with respect to the slab strike, consistent with observations for other deep earthquakes (Wiens, 2001; Tibi et al., 2003), and resulting in different stress drops and radiation efficiencies. However, our sub-event analysis also shows that the first stage of the Bolivia earthquake, although weak, actually had a fast rupture speed, similar to the Okhotsk earthquake and other deep earthquakes in cold slabs. Furthermore, stage 1's rupture direction is also sub-parallel to the local strike of the slab, similar to the Okhotsk earthquake. From this, we infer that the Bolivia earthquake involved two different mechanisms in its two stages, with its first stage being similar to the Okhotsk earthquake except consisting of relatively small amplitude slip. Since the shear melting inferred during the Bolivia earthquake was mostly based on the major rupture parameters dominated by the area with large slip (Kanamori et al., 1998), it is reasonable to assume that the mechanism of stage 2 is shear instability caused by shear melting in a relatively warm slab.

Given our new results, we suggest a conceptual model to explain the different rupture processes of the Bolivia and Okhotsk earthquakes (Fig. 6). Due to the difference in the thermal state of the subducting slabs responsible for the two earthquakes, the predicted widths of the metastable olivine wedges are also different. The Bolivia earthquake nucleated inside the relatively thin cold slab core by the transformational faulting mechanism (Green and Burnley, 1989; Kirby et al., 1991, 1996; Green and Houston, 1995), and ruptured inside the core along slab strike. Due to the small thickness of cold core, the rupture was relatively small but fast. However, after about 10 s, the large sub-event E4 triggered shear melting, allowing the rupture to grow outside the metastable olivine wedge into the warmer slab material, where the melting point is reached more easily (Ogawa, 1987). The positive feedback during shear melting caused the slip to grow rapidly to cause a great earthquake. Due to the substantial energy dissipation involved with shear melting, the rupture speed in this stage decreased significantly. On the other hand, we propose that the recent Okhotsk earthquake nucleated and managed to stay inside the relatively wide metastable olivine wedge in a cold slab. Therefore, the rupture direction stayed close to the slab strike, and the rupture speed stayed relatively high. Interestingly, after the biggest sub-event E2, the rupture also seems to have reset and ruptured both northward and southward, similar to the Bolivia earthquake after its E4, suggesting that very dynamic rupture processes occur during great deep earthquakes. The results shown in this paper demonstrate the complexity of deep earthquakes, and the methodology described has the potential to reveal the mechanics of other earthquakes.

Acknowledgements

We thank Z. Duputel, Q. Zhang and Y. Huang for discussion. The Incorporated Research Institutions for Seismology (IRIS) provided the seismic data. This work is supported by the Tectonic Observatory at California Institute of Technology through GPS.TO2-4.2-Grant.Moore TO2 and is a contribution (#10095) to the Seismological Laboratory, California Institute of Technology.

Appendix A. Supplementary material

Supplementary material related to this article can be found online at http://dx.doi.org/10.1016/j.epsl.2013.10.028.

References

Ammon, C.J., Ji, C., Thio, H.-K., Robinson, D., Ni, S., Hjorleifsdottir, V., Kanamori, H., Lay, T., Das, S., Helmberger, D., 2005. Rupture process of the 2004 Sumatra–Andaman earthquake. Science 308, 1133–1139.

Duputel, Z., Kanamori, H., Tsai, V.C., Rivera, L., Meng, L., Ampuero, J.-P., Stock, J.M., 2012. The 2012 Sumatra great earthquake sequence. Earth Planet. Sci. Lett. 351, 247–257.

Ekström, G., Nettles, M., Dziewoński, A., 2012. The global CMT project 2004–2010: Centroid-moment tensors for 13,017 earthquakes. Phys. Earth Planet. Inter. 200–201, 1–9.

Green II, H., Burnley, P., 1989. A new self-organizing mechanism for deep-focus earthquakes. Nature 341, 733–737.

Green, H.W., Houston, H., 1995. The mechanics of deep earthquakes. Annu. Rev. Earth Planet. Sci. 23, 169–214.

Hayes, G.P., Wald, D.J., Johnson, R.L., 2012. Slab1.0: A three-dimensional model of global subduction zone geometries. J. Geophys. Res. 117, B01302.

Houston, H., 2007. Deep earthquakes. In: Schubert, G. (Ed.), Treatise on Geophysics. Elsevier, Amsterdam, pp. 321–350.

Ihmlé, P.F., 1998. On the interpretation of subevents in teleseismic waveforms: the 1994 Bolivia deep earthquake revisited. J. Geophys. Res. 103, 17919–17932.

International Seismological Centre, 2011. On-line Bulletin. Internatl. Seis. Cent., Thatcham, United Kingdom. http://www.isc.ac.uk.

Ishii, M., Shearer, P.M., Houston, H., Vidale, J.E., 2005. Extent, duration and speed of the 2004 Sumatra–Andaman earthquake imaged by the Hi-Net array. Nature 435, 933–936.

Kanamori, H., Anderson, D.L., Heaton, T.H., 1998. Frictional melting during the rupture of the 1994 Bolivian earthquake. Science 279, 839–842.

Karato, S.-i., Riedel, M.R., Yuen, D.A., 2001. Rheological structure and deformation of subducted slabs in the mantle transition zone: implications for mantle circulation and deep earthquakes. Phys. Earth Planet. Inter. 127, 83–108.

Kikuchi, M., Kanamori, H., 1991. Inversion of complex body waves—III. Bull. Seismol. Soc. Am. 81, 2335–2350.

Kikuchi, M., Kanamori, H., 1994. The mechanism of the deep Bolivia earthquake of June 9, 1994. Geophys. Res. Lett. 21, 2341–2344.

Kirby, S.H., Durham, W.B., Stern, L.A., 1991. Mantle phase changes and deep-earthquake faulting in subducting lithosphere. Science 252, 216–225.

Kirby, S.H., Okal, E.A., Engdahl, E.R., 1995. The 9 June 94 Bolivian deep earthquake: An exceptional event in an extraordinary subduction zone. Geophys. Res. Lett. 22, 2233–2236.

Kirby, S.H., Stein, S., Okal, E.A., Rubie, D.C., 1996. Metastable mantlephase transformations and deep earthquakes in subducting oceanic lithosphere. Rev. Geophys. 34, 261–306.

Meade, C., Jeanloz, R., 1991. Deep-focus earthquakes and recycling of water into the Earth's mantle. Science 252, 68–72.

Myers, S.C., Wallace, T.C., Beck, S.L., Silver, P.G., Zandt, G., Vandecar, J., Minaya, E., 1995. Implications of spatial and temporal development of the aftershock sequence for the Mw 8.3 June 9, 1994 deep Bolivian earthquake. Geophys. Res. Lett. 22, 2269–2272.

Ogawa, M., 1987. Shear instability in a viscoelastic material as the cause of deep focus earthquakes. J. Geophys. Res. 92, 13801–13810.

Persh, S.E., Houston, H., 2004a. Deep earthquake rupture histories determined by global stacking of broadband P waveforms. J. Geophys. Res. 109, B04311.

Persh, S.E., Houston, H., 2004b. Strongly depth-dependent aftershock production in deep earthquakes. Bull. Seismol. Soc. Am. 94, 1808–1816.

Silver, P.G., Beck, S.L., Wallace, T.C., Meade, C., Myers, S.C., James, D.E., Kuehnel, R., 1995. Rupture characteristics of the deep Bolivian earthquake of 9 June 1994 and the mechanism of deep-focus earthquakes. Science 268, 69.

Suzuki, M., Yagi, Y., 2011. Depth dependence of rupture velocity in deep earthquakes. Geophys. Res. Lett. 38, L05308.

Tibi, R., Bock, G., Wiens, D.A., 2003. Source characteristics of large deep earthquakes: Constraint on the faulting mechanism at great depths. J. Geophys. Res. 108, 2091.

Tocheport, A., Rivera, L., Chevrot, S., 2007. A systematic study of source time functions and moment tensors of intermediate and deep earthquakes. J. Geophys. Res. 112, B07311.

Tsai, V.C., Nettles, M., Ekström, G., Dziewonski, A.M., 2005. Multiple CMT source analysis of the 2004 Sumatra earthquake. Geophys. Res. Lett. 32, L17304.

Wei, S., Helmberger, D., Zhan, Z., Graves, R., 2013. Rupture complexity of the Mw 8.3 sea of Okhotsk earthquake: Rapid triggering of complementary earthquakes?. Geophys. Res. Lett. 40, http://dx.doi.org/10.1002/grl.50977.

Wiens, D.A., 2001. Seismological constraints on the mechanism of deep earthquakes: Temperature dependence of deep earthquake source properties. Phys. Earth Planet. Inter. 127, 145–163.

Wiens, D.A., Gilbert, H.J., 1996. Effect of slab temperature on deep-earthquake aftershock productivity and magnitude–frequency relations. Nature 384, 153–156.

Wiens, D.A., McGuire, J.J., 1995. The 1994 Bolivia and Tonga events: Fundamentally different types of deep earthquakes?. Geophys. Res. Lett. 22, 2245–2248.

Ye, L., Lay, T., Kanamori, H., Koper, K.D., 2013. Energy release of the 2013 Mw 8.3 Sea of Okhotsk earthquake and deep slab stress heterogeneity. Science 341, 1380–1384.